KeAi

CHINESE ROOTS
GLOBAL IMPACT

Contents lists available at ScienceDirect

Petroleum Science

journal homepage: www.keaipublishing.com/en/journals/petroleum-science



Original Paper

Multi-stage and multi-objective optimization of anti-typhoon evacuation strategy for riser with new hang-off system



Yan-Wei Li ^a, Xiu-Quan Liu ^{a, b, *}, Peng-Ji Hu ^a, Xiao-Yu Hu ^a, Yuan-Jiang Chang ^{a, b}, Guo-Ming Chen ^{a, b}

- ^a Centre for Offshore Engineering and Safety Technology, China University of Petroleum, Qingdao, 266580, Shandong, China
- b National Engineering Laboratory of Offshore Geophysical and Exploration Equipment, China University of Petroleum, Qingdao, 266580, Shandong, China

ARTICLE INFO

Article history: Received 26 October 2023 Received in revised form 22 June 2024 Accepted 10 September 2024 Available online 11 September 2024

Edited by Teng Zhu and Jia-Jia Fei

Keywords:
Anti-typhoon evacuation strategy
Riser
Multi-stage and multi-objective
Optimization
Genetic algorithm
Least square method

ABSTRACT

A new hang-off system has been proposed to improve the security of risers in hang-off modes during typhoons. However, efficient anti-typhoon evacuation strategies have not been investigated. Optimization model and method for the anti-typhoon evacuation strategies should be researched. Therefore, multi-objective functions are proposed based on operation time, evacuation speed stability, and steering stability. An evacuation path model and a dynamic model of risers with the new hang-off system are developed for design variables and constraints. A multi-objective optimization model with high-dimensional variables and complex constraints is established. Finally, a three-stage optimization method based on genetic algorithm, least square method, and the penalty function method is proposed to solve the multi-objective optimization model. Optimization results show that the operation time can be reduced through operation parameter optimization, especially evacuation heading optimization. The optimal anti-typhoon strategy is evacuation with all risers suspended along a variable path when the direction angle is large, while evacuation with all risers suspended along a straight path at another direction angle. Besides, the influencing factors on anti-typhoon evacuation strategies indicate that the proposed optimization model and method have strong applicability to working conditions and remarkable optimization effects.

© 2024 The Authors. Publishing services by Elsevier B.V. on behalf of KeAi Communications Co. Ltd. This is an open access article under the CC BY-NC-ND license (http://creativecommons.org/licenses/by-nc-nd/4.0/).

1. Introduction

Deepwater drilling risers are essential equipment that connect subsea wellheads and drilling platforms in offshore oil exploration (Bayik et al., 2020; Nguyen and Al-Safran, 2021; Liu et al., 2022b). The safety of risers is seriously threatened by harsh typhoon conditions in the deep sea, especially in the South China Sea where over six typhoons occur each year (Xu et al., 2015; Fan et al., 2017; Yang et al., 2023). To ensure riser safety, connected risers in normal conditions should disconnect from the subsea wellhead under typhoon conditions, thereby forming a recyclable hang-off state (Zhang et al., 2023). Generally, the anti-typhoon evacuation strategy with all risers recovered is implemented. However, risers may not recover during emergency conditions due to inaccurate typhoon forecasts and time delays caused by other operations.

* Corresponding author. E-mail address: lxqmcae@163.com (X.-Q. Liu). Evacuation with the risers in hang-off modes becomes an essential anti-typhoon strategy that is prone to riser failure accidents (Saruhashi et al., 2014; Liu et al., 2017; Wang et al., 2023b). The D534 drilling vessel was affected by Typhoon Prapiroon during a drilling operation in the South China Sea, resulting in a riser fracture accident (Fig. 1(a)). China's offshore oil platform 981 was hit by Typhoon Vicente, causing a collision accident of buoyancy modules (Fig. 1(b)). Furthermore, failure accidents have caused enormous economic losses. Therefore, a safe strategy for evacuation with the risers in hang-off modes must be studied.

The hang-off modes of risers during evacuation can be divided into hard and soft hang-off modes (Liu et al., 2020; Wang et al., 2021). Risers in the soft and hard hang-off modes are hung on the drilling platform via tensioners and directly on the drilling platform, respectively. Some scholars have studied the antityphoon strategies based on the two hang-off modes, including the selection method of the hang-off modes, operation window, and optimum evacuation parameters (Ju et al., 2012; Mao et al.,





(b) Buoyancy modules breaking into collapse

Fig. 1. Failure accidents of risers during typhoon conditions in the South China Sea.

2019; Liu et al., 2022a). The existing research shows that the optimum evacuation parameters, namely, the suspension length of risers, platform evacuation speeds, and platform evacuation heading, are essential for improving the safety of risers (Chen et al., 2012; Qi et al., 2015; Song et al., 2019; Yang and Xiao, 2021). Evacuation with risers in the hard hang-off mode is more dangerous than that in the soft hang-off mode due to the stress concentration of risers (Ambrose et al., 2001; Sun et al., 2009; Xu et al., 2015). Risers in the soft hang-off mode are not adopted in actual anti-typhoon operations for the complex operation procedure and the tensioner stroke limit. A fast and safe riser hang-off mode and suspension equipment must be studied. A safe hangoff mode and suspension equipment with fast response capability must be developed urgently. Therefore, Sheng et al., (2019) proposed a new riser hang-off system with a hang-off joint, centralizer, articulation joint, and supporting device to form a new hard hangoff mode (Fig. 2). The top part of the hang-off joint is hung on a gimbal spider through a supporting device, and the bottom part is connected to risers via the articulation joint. The drilling riser system is composed of a lower flex joint, a series of riser joints, and a lower marine riser package (LMRP) suspended at the bottom of the risers (Liu et al., 2021b). Theoretical research and sea trial testing show that the new riser hang-off system can reduce stress concentration at the top of risers and simplify operational processes (Liu et al., 2021a; Xu et al., 2022; Wang, 2023). However, an efficient and safe method for the utilization of the new hard hangoff mode under typhoon conditions has not been proposed.

The optimal anti-typhoon evacuation strategies for risers in NHHM can be obtained through optimization. It is a typical optimization problem within the domain of offshore oil and gas drilling and completion equipment and operational techniques, while having not been conducted. Some scholars have conducted optimization research on similar problems. Liu et al. (2019) introduced a modified Genetic Algorithm (mGA) tailored for optimizing the configuration of suppression devices in risers. Elsas et al. (2021) developed a Bayesian optimization algorithm, specifically aimed at optimizing steel risers' configuration. Wang et al. (2016) and Adamiec-Wojcik et al. (2023) studied movement optimization method of deepwater risers in the reentry operation. Yang and Xiao (2021) researched an optimization method for the multi-objective optimization of riser operability based on the non-dominated Sorting Genetic Algorithm II (NSGA-II). Most recently, Yang C. et al. (2023) and Yang J. et al. (2023) applied the Global Convergent Method of Moving Asymptotes (GCMMA) for optimization of riser anti-recoil. Among the myriad of optimization techniques,

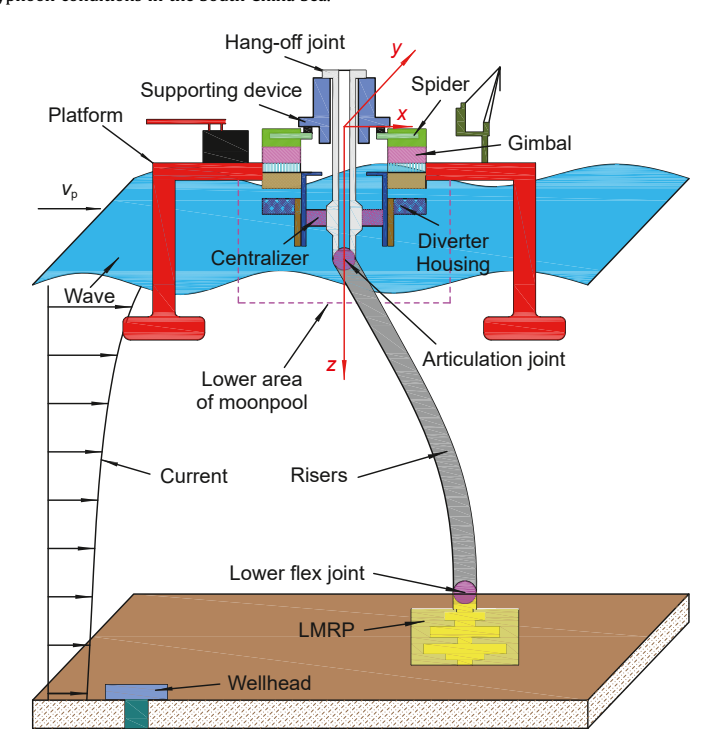


Fig. 2. Deepwater drilling riser in NHHM.

evolutionary algorithms, such as the Genetic Algorithm (GA), Differential Evolution (DE), and Cooperative Co-evolutionary Algorithm (CCEA), have garnered widespread application. This is attributed to their distinct advantages, including robust global search capabilities and exceptional adaptability (Liu et al., 2018; Wang et al., 2023a). Therefore, evolutionary algorithms can be used to optimize anti-typhoon evacuation strategies for risers in NHHM.

The framework of this paper is organized as follows. Section 2 shows a multi-objective optimization model. Section 3 describes a multi-stage optimization method. Section 4 introduces the case study. Section 5 provides the conclusions.

2. Multi-objective optimization model

Fig. 3 shows the anti-typhoon evacuation operations, which includes equipment recovery/installation and evacuation for anti-typhoon. First, a portion of the risers is recovered, and the new

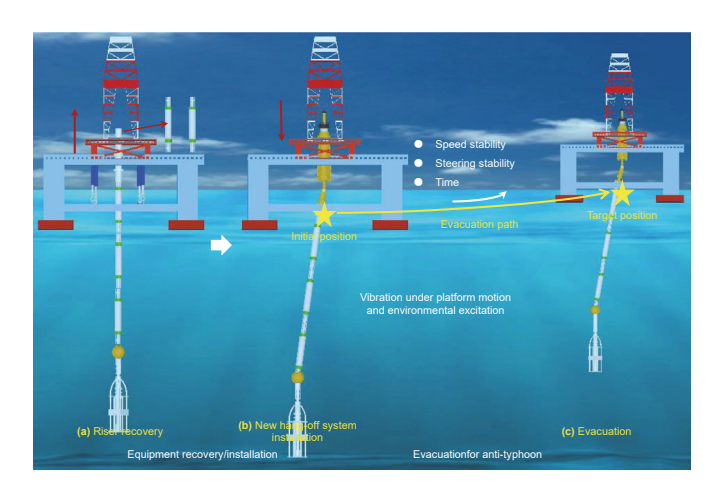


Fig. 3. Anti-typhoon evacuation operations.

hang-off system is installed. Second, the platform evacuates with an evacuation path from the initial to the target position with risers in NHHM. Risers in NHHM vibrates under platform motion and environmental excitation during evacuation. Some operation time is consumed in anti-typhoon evacuation operations, and the operation time is a key indicator for evaluating the effectiveness of the anti-typhoon strategy. The evacuation speed and steering stability of the platform affect the riding comfort of personnel and safety of the riser. Therefore, they are selected as other evaluation indicators.

Anti-typhoon evacuation strategy optimization aims to determine the minimum operation time and the maximum speed and steering stability of the platform. The speed and steering stability can be characterized by the change rate of speed and steering, that is, when the minimum value is optimal. Therefore, the multi-objective optimization model can be expressed as follows (Liu et al., 2019; Monteiro et al., 2021):

opt $\min[f_h(X), f_{tu}(X), f_{ve}(X)]$ s.t. $\begin{cases} h(X) = 0 \\ g(X) \le 0 \end{cases}$ (1

where f_h , f_{tu} , and f_{ve} are objective functions combining the operation time, steering stability, and speed stability, respectively; h and g are the equality and inequality constraints, respectively; and X represents multiple design variables. The objective functions and constraints are listed in Sections 2.1 and 2.2, respectively.

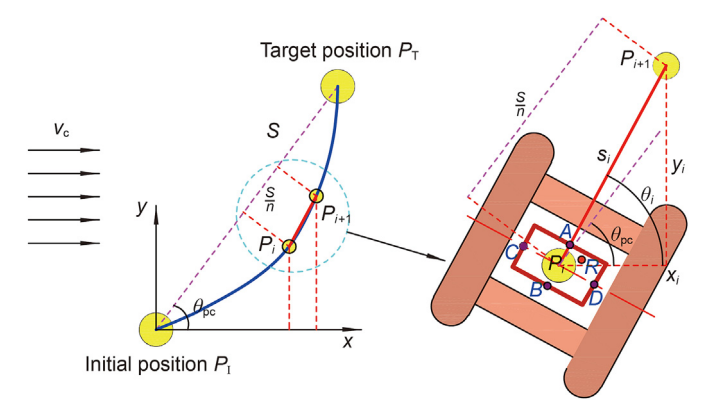


Fig. 4. Evacuation path model.

2.1. Objective functions

An evacuation path model for the drilling platform is proposed to define the steering stability. The speed stability and operation time can be characterized based on the evacuation path model.

2.1.1. Steering stability

The evacuation path is divided into several segments, as shown in Fig. 4. Several coordinate positions of key points that correspond to the segments are defined to build the whole evacuation path.

The platform heading is assumed to be the same as the direction of the evacuation path. The coordinate positions of the initial and target positions are $P_I(0,0)$ and $P_T(S_x, S_y)$, respectively. The coordinate of any coordinate position $P_I(S_{x,j}, S_{y,j})$ can be written as:

$$\begin{cases} S_{x,j} = \sum_{i=1}^{j-1} x_i = \sum_{i=1}^{j-1} s_i \cdot \cos \theta_i \\ S_{y,j} = \sum_{i=1}^{j-1} y_i = \sum_{i=1}^{j-1} s_i \cdot \sin \theta_i \end{cases}$$
 (2)

where j = 2,...,n+1. The straight line P_iP_T is equally divided into n segments, and the length of evacuation path P_iP_{i+1} can be shown as:

$$s_i = \frac{S/n}{\cos|\theta_i - \theta_{DC}|} \tag{3}$$

where θ_{DC} and θ_i are restricted as:

$$\begin{cases}
-90 < \theta_i - \theta_{pc} < 90 \\
0 \le \theta_{pc} < 360
\end{cases}$$
(4)

The total evacuation distances of the platform must satisfy constraints, as shown in Eq. (5).

$$\begin{cases} \sum_{i=1}^{n} s_{i} \cdot \cos \theta_{i} = S \cdot \cos \theta_{pc} \\ \sum_{i=1}^{n} s_{i} \cdot \sin \theta_{i} = S \cdot \sin \theta_{pc} \end{cases}$$
 (5)

Finally, the steering stability f_{tu} is obtained, as shown in Eq. (6).

$$f_{\text{tu}} = \exp\left(\sqrt{\frac{\sum\limits_{i=1}^{n-1} \left(\theta_i^t - \overline{\theta}_i^t\right)^2}{n-1}}\right)$$
 (6)

where the change rate of evacuation heading θ_i^t can be shown as:

$$\theta_i^t = \theta_{i+1} - \theta_i \tag{7}$$

2.1.2. Speed stability

The speed stability f_{ve} can be expressed as:

$$f_{\text{ve}} = \exp\left(\sqrt{\frac{\sum\limits_{i=1}^{n-1} \left(v_i^t - \overline{v}_i^t\right)^2}{n-1}}\right)$$
(8)

2.1.3. Operation time

The operation time wasted in riser recovery/installation can be shown as:

$$T_{da} = N_{R}(N_{j}, N_{b}, N_{L}) \cdot T_{R}(T_{j}, T_{b}, T_{L}) + T_{s}$$
(9)

The time wasted in evacuation $T_{\rm sh}$ can be written as:

$$T_{\rm sh} = \sum_{i=1}^{n} \frac{s_i}{3600 \cdot v_i} \tag{10}$$

Therefore, the time in the overall anti-typhoon evacuation operation can be shown as:

$$f_{\rm h} = T_{\rm sh} + T_{\rm da} \tag{11}$$

The multiple design variables in Eq. (1) are obtained by integrating evacuation headings, speeds, and recovery/installation number of risers, as shown in Eq. (12).

$$X = [N_{R}, \theta_{1}, \theta_{2}, \cdots, \theta_{n}, \nu_{1}, \nu_{2}, \cdots, \nu_{n}]^{T}$$

$$(12)$$

2.2. Constraints

Constraints are composed of the evacuation path, navigation capacity of platform, and strength and physical limits of risers in NHHM. The equality and inequality constraints will be introduced.

2.2.1. Equality constraints

Equality constraints are determined by the evacuation path model in Eq. (5), which can be shown as:

$$\begin{cases} \sum_{i=1}^{n} s_{i} \cdot \cos \theta_{i} - S \cdot \cos \theta_{pc} = 0\\ \sum_{i=1}^{n} s_{i} \cdot \sin \theta_{i} - S \cdot \sin \theta_{pc} = 0 \end{cases}$$
(13)

2.2.2. Inequality constraints

The inequality constraints can be written as (Liu et al., 2017):

$$\begin{cases} a) & -90 < \theta_{i} - \theta_{pc} < 90 \\ b) & 0 < v_{i} \leq v_{p}^{M} \\ c) & N_{R}(N_{j}, N_{b}, N_{L}) \leq N_{R}^{M}(N_{j}, N_{b}, N_{L}) \\ d) & \sigma_{zs,i} \leq \sigma_{zs}^{M} \\ e) & R_{LJ,i} \leq R_{LJ}^{M} \\ f) & R_{AJ,i} \leq R_{AJ}^{M} \\ g) & \mathbf{L}_{P,i} \leq \mathbf{L}_{M,i} \end{cases}$$

$$(14)$$

where i=1,2,...,n; $\mathbf{L}_P \leq \mathbf{L}_P^M$ represents risers that are not allowed to collide with the moonpool. Key points $A(x_a, y_a)$, $B(x_b, y_b)$, $C(x_c, y_c)$, and $D(x_d, y_d)$ on the safety moonpool boundary considering the outer diameter of risers and center point $R(x_p, y_r)$ of the risers near the moonpool are selected, as shown in Fig. 4. The center point R must be located in the enclosed area formed by key points A, B, C, and D for the safety of risers. Therefore, the position constraints can be expressed as Eq. (15).

$$\begin{cases}
D_a + D_b \le D_W - D_R \\
D_c + D_d \le D_L - D_R
\end{cases}$$
(15)

where D_a , D_b , D_c , and D_d are the distance of center point $R(x_r, y_r)$ to the safety moonpool boundary, and they can be written as:

$$\begin{cases} D_{a} = \left| \frac{x_{r}}{\tan \theta_{i}} + y_{r} - \left(\frac{x_{a}}{\tan \theta_{i}} + y_{a} \right) \right| / \sqrt{\left(\frac{1}{\tan \theta_{i}} \right)^{2} + 1} & \theta_{i} \neq 0, \theta_{i} \neq 180, \theta_{i} \neq 90, \theta_{i} \neq 270 \\ D_{a} = |0.5 \cdot (D_{W} - D_{R}) - \operatorname{sign}(\cos \theta_{i}) \cdot x_{r}| & \theta_{i} = 0 \text{ or } \theta_{i} = 180 \\ D_{a} = |0.5 \cdot (D_{W} - D_{R}) - \operatorname{sign}(\sin \theta_{i}) \cdot y_{r}| & \theta_{i} = 90 \text{ or } \theta_{i} = 270 \end{cases}$$

$$\begin{cases} D_{b} = \left| \frac{x_{r}}{\tan \theta_{i}} + y_{r} - \left(\frac{x_{b}}{\tan \theta_{i}} + y_{b} \right) \right| / \sqrt{\left(\frac{1}{\tan \theta_{i}} \right)^{2} + 1} & \theta_{i} \neq 0, \theta_{i} \neq 180, \theta_{i} \neq 90, \theta_{i} \neq 270 \\ D_{b} = |0.5 \cdot (D_{W} - D_{R}) + \operatorname{sign}(\cos \theta_{i}) \cdot x_{r}| & \theta_{i} = 0 \text{ or } \theta_{i} = 180 \\ D_{b} = |0.5 \cdot (D_{W} - D_{R}) + \operatorname{sign}(\sin \theta_{i}) \cdot y_{r}| & \theta_{i} = 90 \text{ or } \theta_{i} = 270 \end{cases}$$

$$\begin{cases} D_{c} = \left| \tan \theta_{i} \cdot x_{r} - y_{r} + (y_{c} - \tan \theta_{i} \cdot x_{c}) \right| / \sqrt{(\tan \theta_{i})^{2} + 1} & \theta_{i} \neq 90 \text{ and } \theta_{i} \neq 270 \\ D_{c} = |0.5 \cdot (D_{L} - D_{R}) + \operatorname{sign}(\sin \theta_{i}) \cdot x_{r}| & \theta_{i} \neq 90 \text{ and } \theta_{i} \neq 270 \\ D_{d} = \left| \tan \theta_{i} \cdot x_{r} - y_{r} + (y_{d} - \tan \theta_{i} \cdot x_{d}) \right| / \sqrt{(\tan \theta_{i})^{2} + 1} & \theta_{i} \neq 90 \text{ and } \theta_{i} \neq 270 \\ D_{d} = \left| (0.5 \cdot (D_{L} - D_{R}) - \operatorname{sign}(\sin \theta_{i}) \cdot x_{r} \right| & \theta_{i} = 90 \text{ or } \theta_{i} = 270 \end{cases}$$

The relative coordinate positions A, B, C, and D to the platform center can be written as:

$$\begin{cases} x_{a} = 0.5 \cdot (D_{W} - D_{R}) \cdot \cos \theta_{i} & y_{a} = 0.5 \cdot (D_{W} - D_{R}) \cdot \sin \theta_{i} \\ x_{b} = -0.5 \cdot (D_{W} - D_{R}) \cdot \cos \theta_{i} & y_{b} = -0.5 \cdot (D_{W} - D_{R}) \cdot \sin \theta_{i} \\ x_{c} = -0.5 \cdot (D_{L} - D_{R}) \cdot \sin \theta_{i} & y_{c} = 0.5 \cdot (D_{L} - D_{R}) \cdot \cos \theta_{i} \\ x_{d} = 0.5 \cdot (D_{L} - D_{R}) \cdot \sin \theta_{i} & y_{d} = -0.5 \cdot (D_{L} - D_{R}) \cdot \cos \theta_{i} \end{cases}$$

$$(17)$$

The response of risers should be obtained through simulation (Liu et al., 2017; Hong et al., 2024). The actual Von Mises stress σ_{zs} and actual rotation angle R_{LJ} in Eqs. (14) and (16) should be calculated by the dynamic analysis of risers in NHHM. Therefore, a dynamic model of risers in NHHM is developed, and the transverse governing differential equations can be written as (Kawano et al., 2021):

among the hang-off joint, diverter housing, and centralizer. The penalty function method is selected because of its convenience in handling contact problems, and the contact force can be shown as:

$$\begin{cases}
F_{\mathsf{C},X}(z) = -k_c \overline{u}_X(z) \\
F_{\mathsf{C},Y}(z) = -k_c \overline{u}_Y(z)
\end{cases}$$
(21)

where k_c is the penalty function that represents the contact stiffness and can be expressed as (Zhang et al., 2020):

$$\begin{cases}
k_{c} = p_{s}k_{s} & l_{t} \leq z \leq l_{b} \\
k_{c} = 0 & \text{else}
\end{cases}$$
(22)

The top of risers in NHHM is hung on the gimbal spider, and the bottom is free. The boundary conditions can be shown as:

$$\begin{cases}
\frac{\partial^{2}}{\partial z^{2}} \left(EI \frac{\partial^{2} u_{x}}{\partial z^{2}} \right) - \frac{\partial}{\partial z} \left(F_{e}(z, t) \frac{\partial u_{x}}{\partial z} \right) + c \frac{\partial u_{x}}{\partial t} + m \frac{\partial^{2} u_{x}}{\partial t^{2}} = F_{W_{-X}}(z, t) + F_{c_{-X}}(z, t) \\
\frac{\partial^{2}}{\partial z^{2}} \left(EI \frac{\partial^{2} u_{y}}{\partial z^{2}} \right) - \frac{\partial}{\partial z} \left(F_{e}(z, t) \frac{\partial u_{y}}{\partial z} \right) + c \frac{\partial u_{y}}{\partial t} + m \frac{\partial^{2} u_{y}}{\partial t^{2}} = F_{W_{-Y}}(z, t) + F_{c_{-Y}}(z, t) \\
\frac{\partial}{\partial z} \left(EA \frac{\partial u_{z}}{\partial z} \right) - c \frac{\partial u_{z}}{\partial t} - m \frac{\partial^{2} u_{z}}{\partial t^{2}} = w_{z}
\end{cases} \tag{18}$$

where F_{e} (N) is the effective axial force of cross-section.

The vibration of risers is affected by internal and external fluids, and the fluid inside risers vibrates with the pipe column (Fan et al., 2017; Yu et al., 2023; Cao et al., 2024). Therefore, the effective axial force that can be written as:

$$F_{e}(z,t) = \begin{cases} \int_{L-z}^{L} w_{z}(z)dz & t = 0\\ EA(z)\frac{\partial u_{z}(z,t)}{\partial z} & t > 0 \end{cases}$$

$$(19)$$

The external lateral hydrodynamic loads on risers are produced by currents. Morison's equation based on empirical and theoretical calculation methods is used widely in engineering and can be shown as (Klaycham et al., 2020; Qu et al., 2023):

$$\begin{cases} \mathbf{u}(0,t) = 0.5H_{\rm p} \cdot \mathbf{A}_{\rm p} \cdot \cos\left(\frac{2\pi}{T_{\rm p}}t - \boldsymbol{\varphi}\right) \\ EI(0) \frac{\partial u_{x}^{2}(0,t)}{\partial z^{2}} = K_{\rm GS}R_{\rm GS_x}, EI(0) \frac{\partial u_{y}^{2}(0,t)}{\partial z^{2}} = K_{\rm GS}R_{\rm GS_y} \end{cases}$$

$$EI(L) \frac{\partial u_{x}^{2}(L,t)}{\partial z^{2}} = EI(L) \frac{\partial u_{y}^{2}(L,t)}{\partial z^{2}} = 0$$

$$(23)$$

Finite element method (FEM) is introduced to solve Eq. (18) for the dynamic analysis of risers in NHHM (Meng et al., 2020). The riser model is discretized into several beam elements, and the finite element equation can be written as Eq. (24). A mechanical solver for the stress, deformation, and rotation of risers is finally developed. The mechanical solver is solved by using the Newmark- β method (Qiu et al., 2023).

$$\mathbf{M}\ddot{\delta} + \mathbf{C}\dot{\delta} + \mathbf{K}\boldsymbol{\delta} = \mathbf{F} \tag{24}$$

$$F_{W_{-X}}(z) = \frac{\pi}{4} \rho_{w} C_{M} D_{h}^{2} \dot{v}_{w} - \frac{\pi}{4} \rho_{w} (C_{M} - 1) D_{h}^{2} \dot{u}_{x} + \frac{1}{2} \rho_{w} D_{h} C_{D} (\nu_{w} + \nu_{c} - \nu_{p} \cdot \cos \theta_{pc} - \dot{u}_{x}) \sqrt{(\nu_{w} + \nu_{c} - \nu_{p} \cdot \cos \theta_{pc} - \dot{u}_{x})^{2} + (-\nu_{p} \cdot \sin \theta_{pc} - \dot{u}_{y})}$$

$$F_{W_{-y}}(z) = -\frac{\pi}{4} \rho_{w} (C_{M} - 1) D_{h}^{2} \dot{u}_{y} + \frac{1}{2} \rho_{w} D_{h} C_{D} (-\nu_{p} \cdot \sin \theta_{pc} - \dot{u}_{y}) \sqrt{(\nu_{w} + \nu_{c} - \nu_{p} \cdot \cos \theta_{pc} - \dot{u}_{x})^{2} + (-\nu_{p} \cdot \sin \theta_{pc} - \dot{u}_{y})}$$

$$(20)$$

where the wave model is Airy's linear wave theory.

A complex contact problem is generated by the relationship

where ${\it M}$ is the mass matrix, ${\it C}$ is the damping matrix, ${\it K}$ is the

stiffness matrix, δ is the displacement vector, and ${\bf \it F}$ is the load vector.

3. Multi-stage optimization method

3.1. Equivalent conversion method

The established optimization model of the anti-typhoon evacuation strategy exhibits the characteristics of multi-objective and complex constraints, which makes it difficult to obtain the optimal solution. Constraints and multi-objective functions need to be further processed.

3.1.1. Constraints

The equality constraints in Eq. (13) show the relationship between the platform heading and evacuation distance. The design variable θ_n in Eq. (12) is treated as a dependent variable, and it can be written as:

shown as:

$$\gamma = \frac{p_b \cdot S}{n} \tag{28}$$

where p_b is the reference adjustment ratio, dimensionless.

The comprehensive penalty item for all inequality constraints is written as:

$$\phi = \sum_{i=1}^{n} \left(\phi_{ZS,i} + \phi_{LJ,i} + \phi_{AJ,i} + \phi_{X,i} + \phi_{y,i} \right)$$
 (29)

The additive operation time is established by combining the comprehensive penalty item and the actual operation time, as expressed in Eq. (30).

$$f_{\rm h} = T_{\rm sh} + T_{\rm da} + \phi \tag{30}$$

$$\theta_{n} = \arcsin\left(\frac{\left(S \cdot \sin \theta_{pc} - \sum_{i=1}^{n-1} s_{i} \cdot \sin \theta_{i}\right)}{\sqrt{\left(S \cdot \cos \theta_{pc} - \sum_{i=1}^{n-1} s_{i} \cdot \cos \theta_{i}\right)^{2} + \left(S \cdot \sin \theta_{pc} - \sum_{i=1}^{n-1} s_{i} \cdot \sin \theta_{i}\right)^{2}}}\right)$$
(25)

where the value range of θ_n is -90 to 270. Besides, the multiple design variables in Eq. (12) degenerate to Eq. (26).

$$X = [N_{R}, \theta_{1}, \theta_{2}, \cdots, \theta_{n-1}, \nu_{1}, \nu_{2}, \cdots, \nu_{n}]^{T}$$
(26)

The inequality constraints a)–c) are the value range of the multiple design variables that do not need to be processed, whereas the inequality constraints d)–g) must be dealt with. The penalty function method is introduced to deal with inequality constraints, and penalty terms $(\phi_{zs,i}; \phi_{IJ,i}; \phi_{AJ,i}, \phi_{x,i}, \phi_{y,i})$ for the inequality constraints d)–g) can be written as (Ja'e et al., 2022):

$$\begin{split} & \text{d1)} \ \phi_{zs,i} \! = \! \begin{cases} 0 & \sigma_{zs,i} \! \le \! \sigma_{zs}^M \\ \gamma \! \cdot \! \left[\left(\sigma_{zs,i} \! - \! \sigma_{zs}^M \right) \! \cdot \! \gamma_{zs} \right]^{\lambda} & \sigma_{zs,i} \! > \! \sigma_{zs}^M \\ & \text{e1)} \ \phi_{LJ,i} \! = \! \begin{cases} 0 & R_{LJ,i} \! \le \! R_{LJ}^M \\ \gamma \! \cdot \! \left[\left(R_{LJ,i} \! - \! R_{LJ}^M \right) \! \cdot \! \gamma_{LJ} \right]^{\lambda} & R_{LJ,i} \! > \! R_{LJ}^M \\ & \text{f1)} \ \phi_{AJ,i} \! = \! \begin{cases} 0 & R_{AJ,i} \! \le \! R_{AJ}^M \\ \gamma \! \cdot \! \left[\left(R_{AJ,i} \! - \! R_{AJ}^M \right) \! \cdot \! \gamma_{AJ} \right]^{\lambda} & R_{AJ,i} \! > \! R_{AJ}^M \\ & \phi_{x,i} \! = \! \begin{cases} 0 & D_a \! + \! D_b \! \le \! D_W \! - \! D_R \\ \gamma \! \cdot \! \left[\left(D_a \! + \! D_b \right) \! - \! \left(D_W \! - \! D_R \right) \right] \! / 2 \! \cdot \! \gamma_x \}^{\lambda} & D_a \! + \! D_b \! > \! D_W \! - \! D_R \\ g1) & \phi_{y,i} \! = \! \begin{cases} 0 & D_c \! + \! D_d \! \le \! D_L \! - \! D_R \\ \gamma \! \cdot \! \left\{ \left[\left(D_c \! + \! D_d \right) \! - \! \left(D_L \! - \! D_R \right) \right] \! / 2 \! \cdot \! \gamma_y \right\}^{\lambda} & D_c \! + \! D_d \! > \! D_L \! - \! D_R \\ \end{cases} \end{split}$$

where, γ (dimensionless) is an adjustment proportion that corresponds to a different number of design variables, which can be

3.1.2. Multi-objective function

The complex multi-objective model is transformed into a single-objective equivalent model with strong solving ability by weighing multiple objectives (Wu et al., 2021; Zheng et al., 2023). The single-objective equivalent function can be expressed as:

$$U(X) = \omega_{1} \frac{(f_{h}(X) - f_{h}(X_{1}^{*}))}{f_{h}(X_{1}^{*})} + \omega_{2} \frac{(f_{tu}(X) - f_{tu}(X_{2}^{*}))}{f_{tu}(X_{2}^{*})} + \omega_{3} \frac{(f_{ve}(X) - f_{ve}(X_{3}^{*}))}{f_{ve}(X_{2}^{*})}$$
(31)

where $f_h(X_1^*)$, $f_{tu}(X_2^*)$, and $f_{ve}(X_3^*)$ are the optimal solutions of each single objective in the feasible region. The relationship of weight coefficients ω_1 , ω_2 , and ω_3 needs to meet Eq. (33).

$$\begin{cases} \omega_1 \geq 0, \omega_2 \geq 0, \omega_3 \geq 0 \\ \omega_1 + \omega_2 + \omega_3 = 1 \end{cases}$$
 (32)

3.2. Optimization method

The objective function for the multi-objective optimization model is relevant to platform evacuation speed, evacuation heading, and riser configuration, thereby causing the multi-objective optimization model to have strong nonlinearity. The design variables have higher dimensions for improving the platform evacuation stability and anti-typhoon operational efficiency. Obtaining globally optimal solutions is extremely difficult. Besides, the dynamic analysis of risers is time-consuming, thereby making the optimal solution inefficient.

Multi-stage optimization solution methods are suitable for solving this challenge because the design variables can be divided

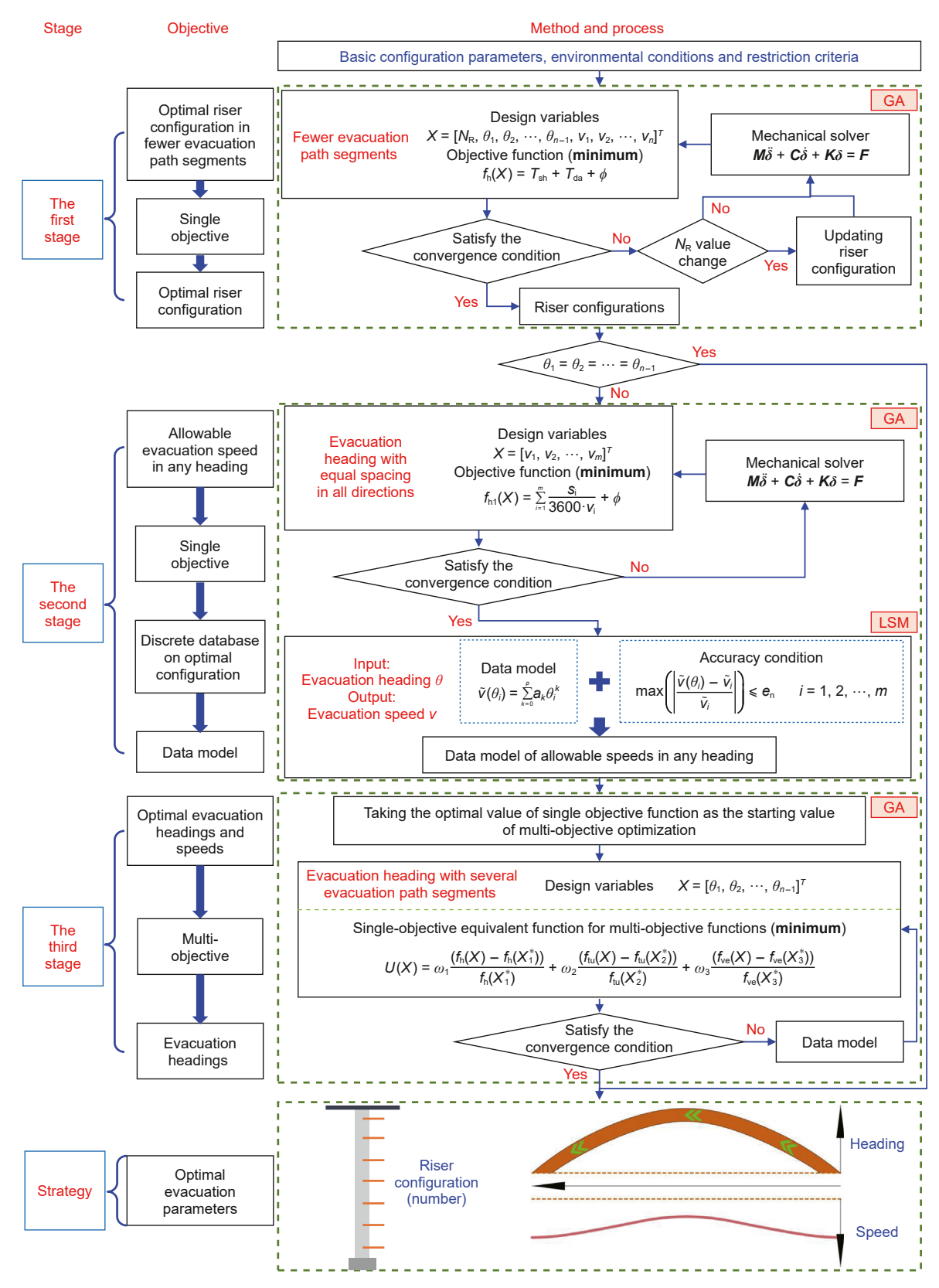


Fig. 5. Flow chart of the three-stage optimization method.

into several groups optimized in stages (Yan et al., 2019; Bakker et al., 2020; Ahmed and Demirci, 2022). An optimal riser configuration can be determined by the global optimization of the single operation time function. Allowable evacuation speeds on any evacuation heading can be designed under the optimal riser configuration. Finally, the optimal evacuation heading can be optimized. Therefore, the optimization solution process can be divided into three stages, with optimization objectives for riser configuration, platform evacuation speeds, and evacuation headings, respectively.

The common challenge in these three stages is which optimization algorithm to choose. GA is a random global search and optimization method with high efficiency, parallelizability, and global search (Dou et al., 2022; Sinha et al., 2023). Therefore, it is chosen as the basic optimization algorithm. A small discrete database of platform allowable evacuation speed for the determinant riser configuration can be established in the second stage, but it cannot be directly used in the optimization process under the third stage. The least square method (LSM) is convenient and efficient for establishing a data model for a small discrete database. The data model can be expressed as Eq. (33) for the evacuation heading and allowance evacuation speed that satisfies a one-to-one function (Gong et al., 2021; Yu et al., 2022).

$$\tilde{v}(\theta_i) = \sum_{k=0}^{p} a_k \theta_i^k \tag{33}$$

The fitting degree between the data model and the data can be expressed as:

$$S_{V}(a_{0}, a_{1}, \dots, a_{p}) = \sum_{i=1}^{m} \left(\sum_{k=0}^{p} a_{k} \theta_{i}^{k} - \tilde{v}_{i} \right)^{2}$$
(34)

where S_V is the loss function, dimensionless; and m is the number of discrete database, dimensionless. The fitting degree is highest when S_V reaches its minimum value, and S_V meets Eq. (35).

$$\frac{\partial S_{\mathbf{v}}(a_0, a_1, \dots, a_p)}{\partial a_k} = 0 \quad k = 0, 1, \dots, p$$
(35)

The highest order of the data model is determined by Eq. (36).

$$\max\left(\left|\frac{\tilde{v}(\theta_i) - \tilde{v}_i}{\tilde{v}_i}\right|\right) \le e_n \qquad i = 1, 2, \dots, m$$
(36)

where e_n is the value of control error, dimensionless.

A three-stage optimization method based on GA and LSM is proposed for the global optimal solution of the multi-objective optimization model, and it is also developed based on MATLAB. The flow chart of the three-stage optimization method is shown in Fig. 5. Basic configuration parameters, environmental conditions, and restriction criteria of risers in NHHM are first confirmed. Then, the solution process is described.

Table 1 Wave and current data.

Wave											
Wave height, m Period, s											10.2 13.5
Current											
Water depth from surface, m Current velocity, m/s	0 1.37	25 1.32	247 0.95	411 0.59	576 0.59	740 0.58	904 0.57	1069 0.56	1233 0.56	1398 0.56	1 m above seabed 0.34

Table 2 Hydrodynamic properties.

Property	Symbol	Value
Drag coefficient	C_{D}	1.2 (down to 150 m below mean sea level (MSL)) 0.7 (between 150 m below MSL and seabed)
Inertia coefficient	C_{M}	2.0 (at all depths)

- (1) The first stage is to obtain the optimal riser configuration through fewer evacuation path segments. The riser number, evacuation heading, and speed are selected as design variables. The anti-typhoon operation time is optimized by GA by selecting the operation time function as the sole optimization objective. The optimal anti-typhoon evacuation strategy will be achieved in the first stage when all evacuation headings are consistent.
- (2) The second stage is to gain allowable evacuation speed in any evacuation heading. An objective function of evacuation time with constraints on several directions is established. GA is used to obtain a discrete database of allowable evacuation speeds for the optimal riser configuration. A data model on allowable evacuation speeds is trained based on LSM.
- (3) The third stage is to design the optimal evacuation headings and speeds. The evacuation headings are selected as design variables because the evacuation speeds can be obtained through the data model. The single-objective equivalent function *U*(*X*) is optimized based on GA that the optimal evacuation headings obtained.

Finally, an optimal anti-typhoon evacuation strategy with evacuation headings, evacuation speeds, and riser configuration is designed.

4. Case study

Some engineering cases are selected for the optimization of anti-typhoon evacuation strategies. A deepwater semi-submersible platform in the South China Sea is selected, as shown in Fig. 1. The wave and current data and hydrodynamic properties of risers are listed in Tables 1 and 2, respectively. The hang-off joint and riser parameters are listed in Tables 3 and 4, respectively. Optimization and structural parameters are listed in Table 5. RAOs of the platform are shown in Fig. 6, and other data have been omitted due to their huge amount. The height of the moonpool from the mean sea level is 10 m.

4.1. Optimal analysis

A riser configuration of 1500 m with 65 risers is selected for the characteristic analysis of anti-typhoon evacuation strategies. The linear distance between the initial and the target positions is 18520 m (10 n mils). The direction angle are 0° , 90° , 135° , 150° , 165° , and 180° .

Table 3 Hang-off joint parameters.

Segment length, m	External diameter, mm	Internal diameter, mm	Remarks
4.55	203.2	88.9	
2.24	203.2	0	
0.19	228.6	0	
0.8	393.7	0	Centralizer
0.596	393.7	0	
0.298	368.3	0	
0.298	342.9	0	
0.298	317.5	0	

Table 4Riser parameters.

Components	Unit length, m	Hydrodynamic external diameter, m	Dry weight, kg	Wet weight, kg
Hang-off joint	_	_	_	_
Articulation joint	1.82	0.5	2200	1500
21" × 1" riser joint	22.86	0.5334	17584.4	15298.3
$21" \times 1"$ riser joint w/2500 ft buoyancy	22.86	1.3716	23365.75	781
21" \times 0.9375" riser joint w/2500 ft buoyancy	22.86	1.3716	23000.8	330.2
$21" \times 0.875"$ riser joint w/5000 ft buoyancy	22.86	1.3716	24279.9	1660.1
$21" \times 0.875"$ riser joint w/7500 ft buoyancy	22.86	1.3716	24463.6	1843.9
$21" \times 0.75"$ riser joint w/10000 ft buoyancy	22.86	1.3716	24749.8	2164.1
Lower flex joint	2.074	1.3716	13608	12000
LMRP	6.1	5.5	120000	104331

Table 5Optimization and structural parameters.

Parameter symbols	$T_{\rm j}$	$T_{\rm b}$	$T_{\rm L}$	$T_{\rm s}$	ω_1	ω_2	ω_3	$p_{ m b}$
Value	0.5	0.5	2.5	3	0.6	0.2	0.2	4
Parameter symbols	γ_{zs}	γ _{LJ}	γ_{AJ}	γ_x	γ_y	λ	D_{W}	$D_{ m L}$
Value	0.5	30	30	6	6	1	7.6	39.4
Parameter symbols	K_{GS}	K_{LJ}	R_{AJ}^{M}	$R_{\rm LJ}^{\rm M}$	$v_{\rm p}^{\rm M}$	$\sigma_{ m zs}^{ m M}$	p_{s}	
Value	340280	127400	30	9	1.543	370	0.01	

4.1.1. First stage

The number of design variables is eight. The population size, crossover probability, and compilation probability are 300, 0.95, and 0.05, respectively. The convergence curves of the fitness value in 90° and 180° direction angles are shown in Fig. 7. The convergence solution can be obtained within 200 generations, indicating that the optimization method has good convergence. The optimization results indicate that evacuation with all risers suspended consumes the least operating time, as listed in Table 6. Evacuation headings also need to be optimized when direction angles are 150°, 165°, and 180°. The reason is that the current force on risers

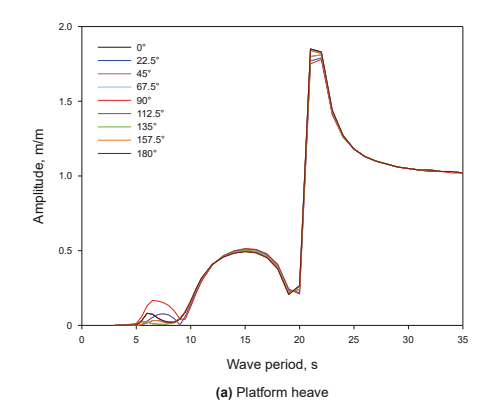
increases with the direction angle, thereby lowering the allowable evacuation speed of the platform. However, the time wasted in riser recovery/installation is still greater than that saved by the evacuation speed improvement.

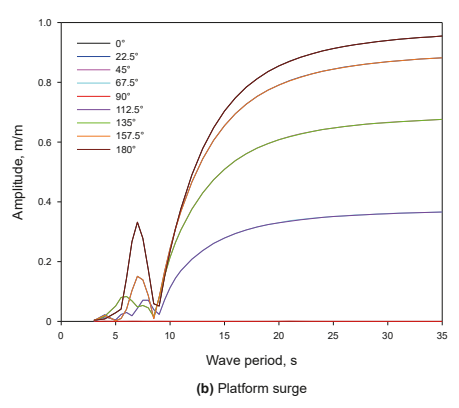
4.1.2. Second stage

The optimization variables of evacuation heading are designed at intervals of 10° from 0° to 180°. The population size, crossover probability, and compilation probability are 400, 0.95, and 0.05, respectively. A discrete database for allowable evacuation speed is obtained through speed optimization. A data model based on the discrete database is established by data training, and the highest order is five. Fig. 8 shows the comparison result between data from the data model and the discrete database. The data model has good accuracy with errors below 0.88%, thereby meeting the needs of optimization design in the third stage, as shown in Fig. 9.

4.1.3. Third stage

The evacuation path is divided into 40 segments, and the design variable number for evacuation headings is 39. The population size, crossover probability, and compilation probability are 500, 0.97,





 $\textbf{Fig. 6.} \ \ \text{RAOs of the platform.}$

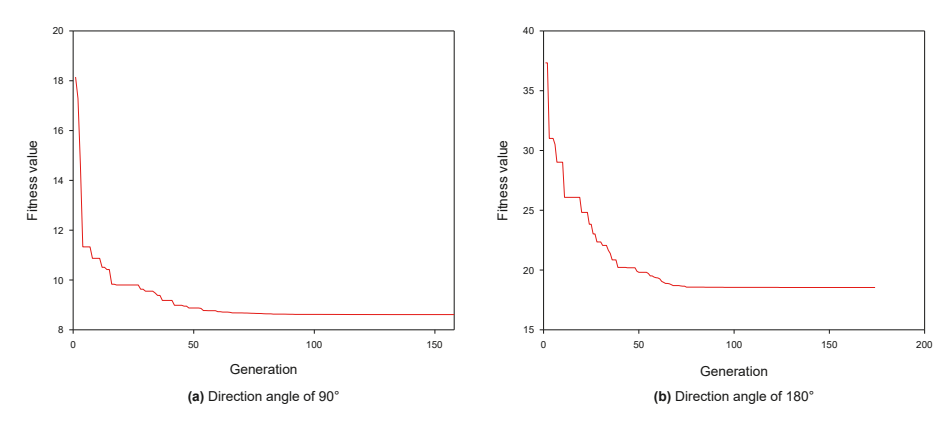


Fig. 7. Convergence curves of the operation time.

Table 6 Optimal riser configurations.

Direction angle $\theta_{ m pc}$	0	90	135	150	165	180
Optimal riser configuration	All	risers s	uspended	1		
Consistent evacuation heading	Yes			No		

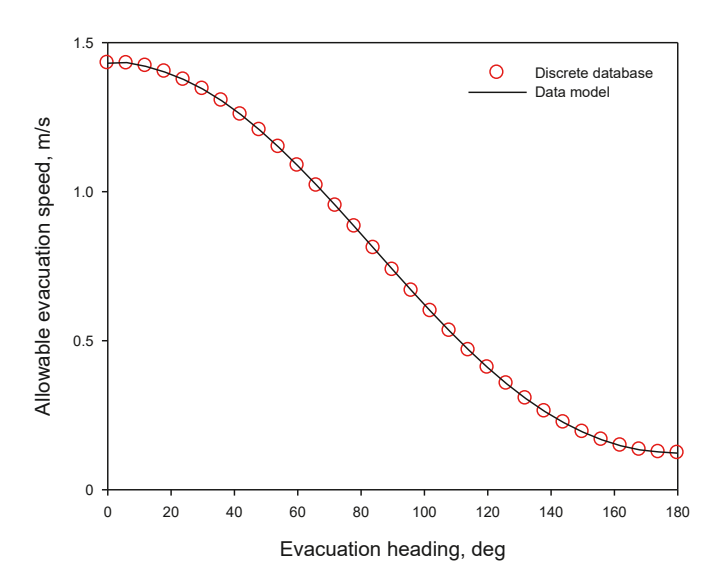


Fig. 8. Comparison result.

and 0.03, respectively. The optimal solution is obtained after 428 generations with the convergence curve of fitness value shown in Fig. 10. The optimization results show that the optimal evacuation strategies in large direction angles are reducing the angle between evacuation heading and current for improving evacuation speed, as shown in Figs. 11 and 12. The operation time can be saved through strategy optimization, especially evacuation heading optimization, which includes configuration optimization and evacuation speed optimization, as shown in Fig. 13. In this figure, "None", "Configuration only", and "Heading" represent no optimization, configuration optimization only, both configuration and evacuation speed optimization, respectively. Besides, the bar chart and line chart represent the operation and saving rate, respectively. It is shown that the heading optimization has advantages compared with the configuration optimization only in the large direction angle, and the saving rate of operation time is increased by more than 20% when the direction angle is 180°. However, the time saved

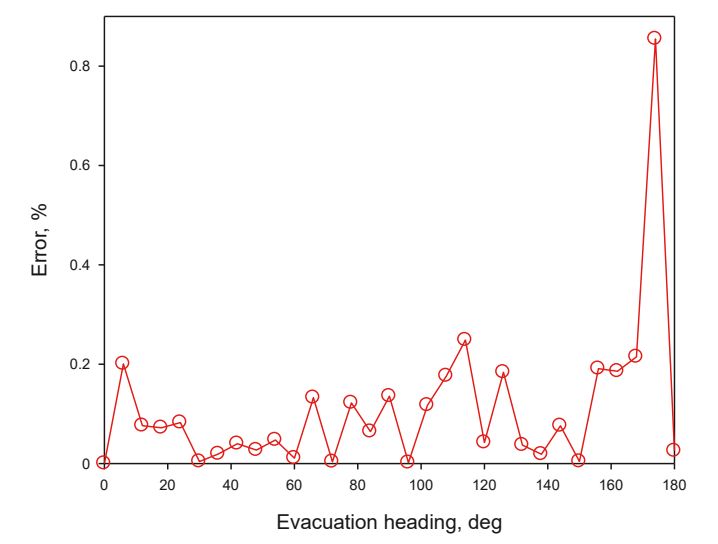


Fig. 9. Errors of the data model.

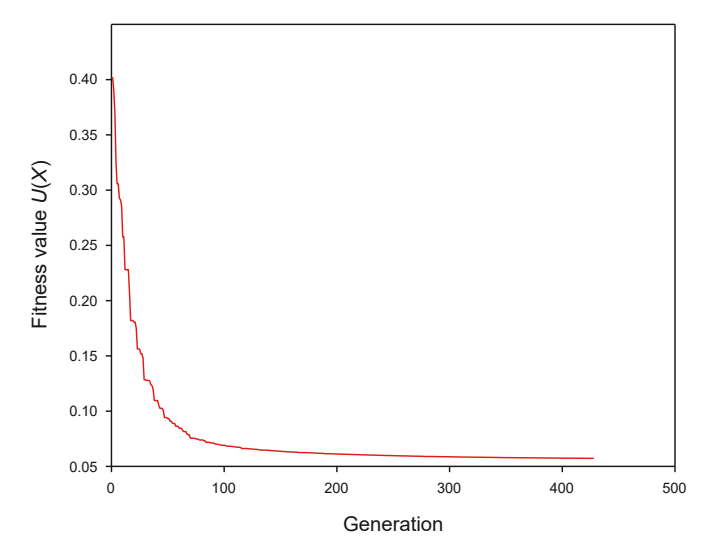


Fig. 10. Convergence curve of fitness value.

decreases as the direction angle increases. The reason is that the time wasted in evacuation decreases with the rise in allowance evacuation speed. Then, the operation time can be reduced by

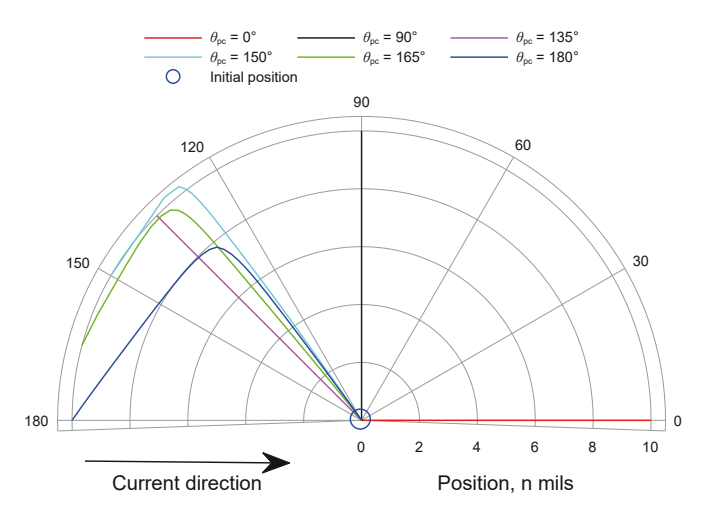


Fig. 11. Optimal evacuation heading.

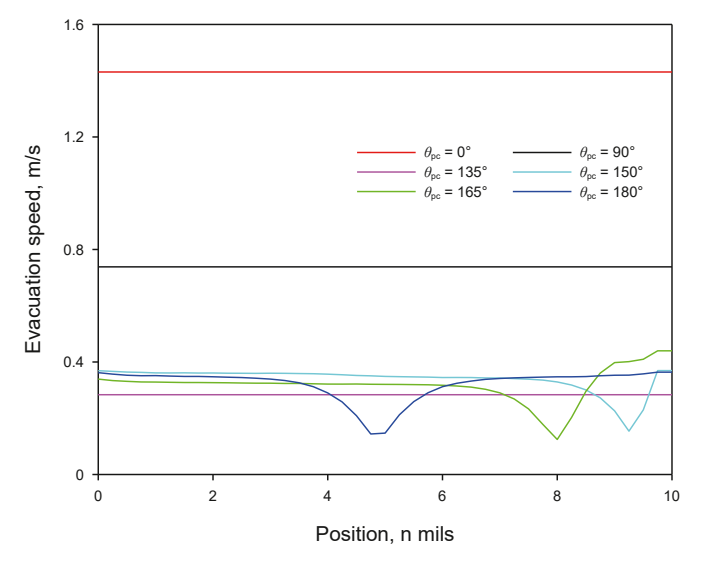


Fig. 12. Optimal evacuation speed.

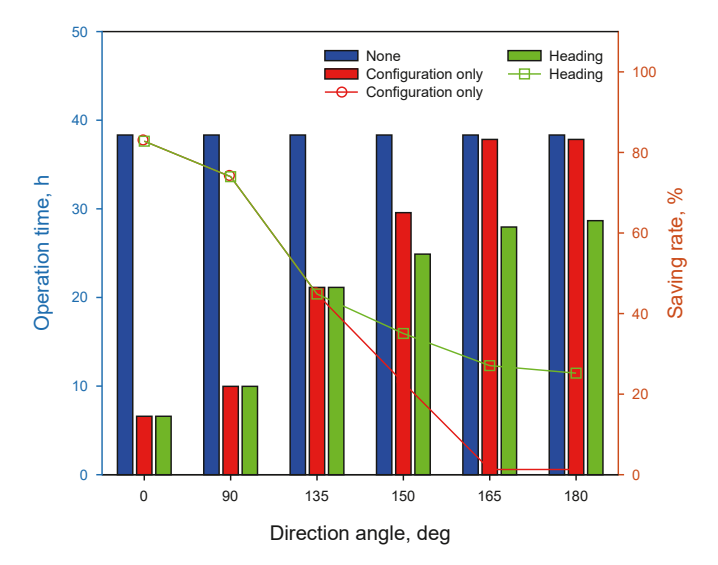


Fig. 13. Operation time.

Table 7 Anti-typhoon evacuation strategies.

Strategy mode	Evacuation operation method
Strategy A	Evacuation with all risers suspended along a straight path
Strategy B	Evacuation with all risers suspended along a variable path
Strategy C	Evacuation with two risers suspended along a straight path

reducing the angle between the evacuation heading and the current direction.

4.2. Influencing factor analysis

The current velocity (surface current velocity), wave height, wave period, and water depth may influence anti-typhoon evacuation strategies. Thus, some cases of influencing factors on anti-typhoon operation strategies are analyzed. Three anti-typhoon evacuation strategies are identified, as listed in Table 7. The basic environment condition and riser configuration are the same as those presented in Section 5.1.

Fig. 14 shows the anti-typhoon evacuation strategies and the time saved for a riser configuration of 1500 m in various surface current velocities. The optimal evacuation strategy gradually shifts from strategy A to B and C as the surface current velocity and direction angle increase. The reason is that the operation time wasted in riser recovery/installation sharply increases with the surface current velocity and direction angle, and the time saved decreases at the same time, as shown in Fig. 14(b). The advantage of evacuation with all risers suspended is reduced.

Figs. 15 and 16 show the anti-typhoon evacuation strategies and the time saved for a riser configuration of 1500 m in various wave heights and wave periods, respectively. The time saved decreases almost linearly with wave height and wave period, while it sharply decreases with direction angle, as shown in Figs. 15(b) and 16(b). Therefore, the impact of direction angle on evacuation strategies is greater than that of wave height and period. The optimal operational strategy is evacuation with all risers suspended along a straight path when the direction angle is less than 130°, otherwise the evacuation heading should be optimized.

Fig. 17 shows the anti-typhoon evacuation strategies and the time saved in various water depths. The time saved increases almost linearly with water depth, while it sharply decreases with direction angle, as shown in Fig. 17(b). Besides, the time saved is almost zero in an area with direction angles greater than 130° and water depths less than 1000 m. Therefore, the optimal evacuation strategy is evacuation with two risers suspended along a straight path in that area. The evacuation strategies in other areas are consistent with the analysis results under influencing factors of wave height and wave period.

The proposed method has strong applicability to working conditions and remarkable optimization effects. A conclusion is that the time saved decreases with the increase in direction angle. Besides, the time saved decreases with the increase in surface current velocity, wave height, and wave period and rises with water depth. Additionally, the relationship between the time wasted in evacuation and influencing factors can elucidate that the operation time is reduced by changing the evacuation heading in a high direction angle.

5. Conclusions

This paper focuses on a complex issue, that is, the development of a comprehensive optimization model and optimization method for the anti-typhoon evacuation strategy. The operation time,

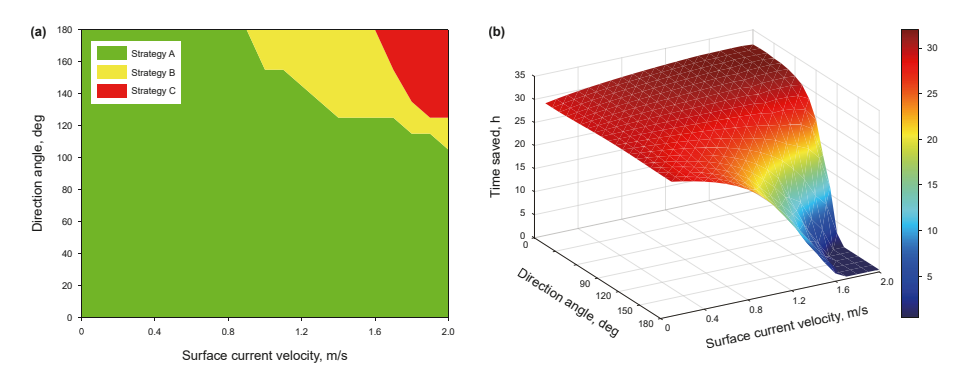


Fig. 14. Optimization results in various surface current velocities.

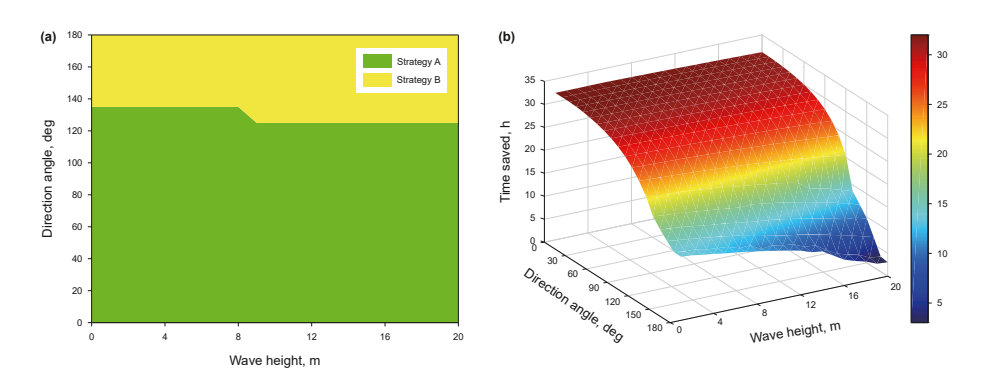


Fig. 15. Optimization results in various wave heights.

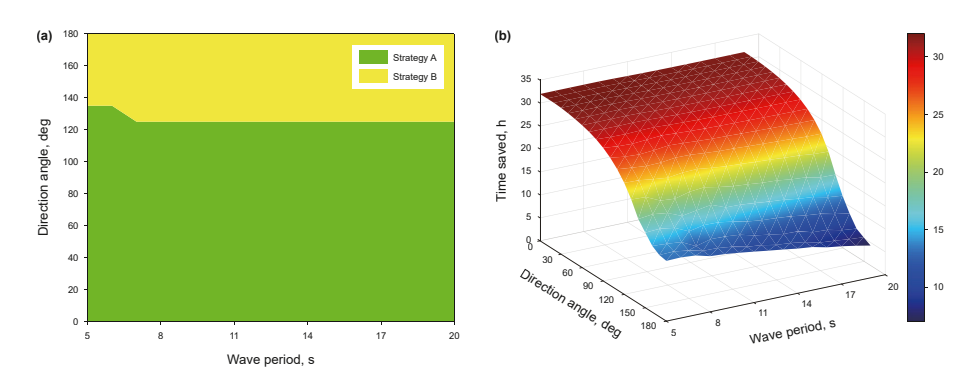
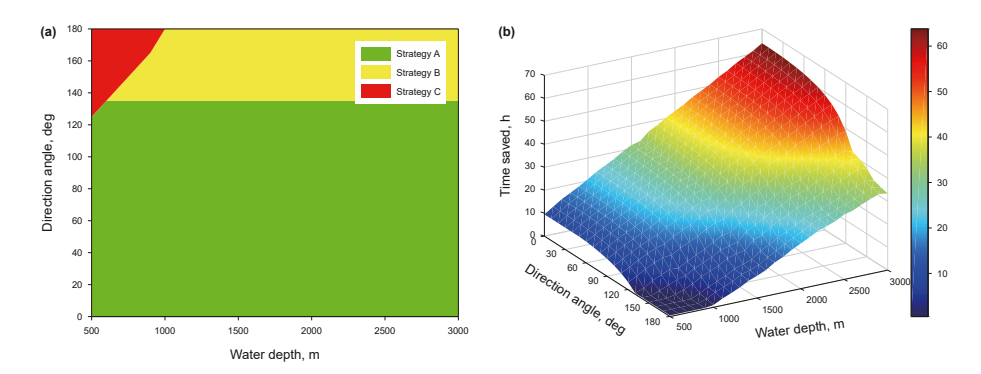


Fig. 16. Optimization results in various wave periods.



 $\textbf{Fig. 17.} \ \ \textbf{Optimization results in various water depths.}$

evacuation speed stability, and steering stability of the platform are selected as multi-objective functions. An evacuation path model and a dynamic model of risers in NHHM are introduced to build constraints. Design variables are formed by integrating evacuation headings, speeds, and riser configurations. Finally, a multi-objective optimization model of the anti-typhoon evacuation strategy is established based on the objective functions, constraints, and design variables.

The multi-objective optimization model with high-dimensional variables and complex constraints is handled by the penalty function method and weighing multiple objectives. A three-stage optimization method based on GA and LSM is proposed for the global optimal solution. In the first stage, an optimal riser configuration is determined through fewer evacuation path segments based on GA. Then, a data model on allowable evacuation speeds for the optimal riser configuration is established based on GA and LSM. Finally, optimal evacuation headings and speeds are optimized based on GA by combining the data model and the singleobjective equivalent function.

The proposed method is applied in anti-typhoon evacuation strategy optimization for risers in NHHM. The proposed optimization model and method efficiently perform the optimization design of the anti-typhoon evacuation strategy. The operation time can be reduced by strategy optimization, especially the evacuation heading optimization, which includes configuration optimization and evacuation speed optimization. The optimal anti-typhoon strategy suspended all risers along a variable path when the direction angle is large and suspended all risers along a straight path in other direction angles. Besides, the results of influencing factors on antityphoon evacuation strategies indicate that the proposed method has strong applicability to working conditions and has remarkable optimization effects.

CRediT authorship contribution statement

Yan-Wei Li: Writing - original draft. Xiu-Quan Liu: Methodology. Peng-Ji Hu: Software. Xiao-Yu Hu: Validation. Yuan-Jiang **Chang:** Writing – review & editing. **Guo-Ming Chen:** Writing – review & editing.

Declaration of competing interest

The authors declare that they have no known competing financial interests or personal relationships that could have appeared to influence the work reported in this paper.

Acknowledgements

This work was supported by the National Natural Science Foundation of China (Grant No: 52271300, 52071337), National Key Research and Development Program of China (2022YFC2806501), High-tech Ship Research Projects Sponsored by MIIT (CBG2N21-4-25), Program for Changjiang Scholars and Innovative Research Team in University (Grant No. IRT14R58).

Nomenclature

θ_i	platform evacuation heading, deg
S	linear distance between the initial and target position, m
θ_{pc}	direction angle, deg
$\hat{v_i}$	platform evacuation speed, m/s
N_{R}	recovery/installation number of risers, dimensionless
$T_{\mathbf{R}}$	recovery/installation time of a single one, h
$T_{\rm j}$	recovery/installation time of the slick joint, h
$T_{\mathbf{b}}$	recovery/installation time of the buoyancy joint, h
$T_{\rm L}$	recovery/installation time of LMRP, h
$N_{\rm j}$	recovery/installation number of the slick joint, dimensionless
$N_{\rm b}$	recovery/installation number of the buoyancy joint, dimensionless
$N_{\rm L}$	recovery/installation number of LMRP, dimensionless
T_{s}	recovery/installation time of the new hang-off system, h
$N_{ m R}^{ m M}$	number of riser configuration when risers are disconnected, dimensionless
$v_{\rm p}^{\rm M}$	allowable speed of platform, m/s
σ_{ZS}	actual Von Mises stress of risers, MPa
$\sigma_{ m zs}^{ m M}$	allowable Von Mises stress of risers, MPa
R _{LI}	actual rotation angle of the lower flex joint, deg
$R_{\rm LI}^{ m M}$	allowable rotation angle of the lower flex joint, deg
R _{AI}	actual rotation angle of the articulation joint, deg
R _{AI}	allowable rotation angle of the articulation joint, deg
•	
D_{W}	width of the moonpool, m
$D_{\rm L}$	length of the moonpool, m diameter of the risers near the moonpool, m
D_{R}	vertical coordinate of risers, m
Z	lateral deformation of risers in the x direction, m
u_{x}	lateral deformation of risers in the x direction, m
$u_{y,}$	lateral deformation of risers in the z direction, m
u _z E	Young's modulus, Pa
E I	rotational inertia. m ⁴
C	damping coefficient, kg/(m·s)
m	total mass per unit riser length, kg/m
F _{c x}	unit length contact force by the centralizer in the x direction, N
$F_{c,v}$	unit length contact force by the centralizer in the x direction, N
F _{C_y}	lateral hydrodynamic loads on unit length risers in the x direction, N
$F_{\mathbf{W},\mathbf{y}}$	lateral hydrodynamic loads on unit length risers in the y direction, N
r _{W_y}	iateral hydrodynamic loads on dint length fisers in the y direction, in

(continued)	
w_z	wet weight on unit length risers with internal fluid, N
L	total length of risers and the new hang-off joint, m
$ ho_{W}$	seawater density, kg/m³
$D_{ m h}$	hydrodynamic outer diameter of risers, m
$C_{\mathbf{M}}$	inertia coefficients, dimensionless
C_{D}	drag coefficients, dimensionless
$v_{\rm c}$	current steady-state flow velocity, m/s
$v_{\sf w}$	water particle velocity in the lateral direction, m/s
\dot{v}_{W}	water particle acceleration in the lateral direction, m/s 2
$v_{ m p}$	platform evacuation speed, m/s
$\overline{u}_{x}(z)$	relative lateral deformation of the hang-off joint at the diverter housing in the x direction, m
$\overline{u}_{y}(z)$	relative lateral deformation of the hang-off joint at the diverter housing in the y direction, m
p_{s}	penalty factor, dimensionless
k _s	related to the contact body, N/m
l_{t}	distance from the top of the hang-off joint to the top of the centralizer, m
$l_{\mathbf{b}}$	distance from the top of the hang-off joint to bottom of the centralizer, m
K_{GS}	rotational stiffness of the gimbal spider, N \cdot m/rad
R_{GS_X}	relative rotation angles of the gimbal spider in the x direction, rad
R_{GS_y}	relative rotation angles of the gimbal spider in the y direction, rad
$\boldsymbol{u}(0,t)$	platform motion on six degrees-of-freedom by waves
$A_{ m p}$	response amplitude, m/m (deg/m, deg)
$H_{\rm p}$	amplitude of regular wave, m
$T_{\mathbf{p}}$	wave period, s
$oldsymbol{arphi}$	phase difference between the platform motion and waves, deg
λ	growth index of the penalty function, dimensionless
$\gamma_{\rm ZS}$, $\gamma_{\rm LJ}$, $\gamma_{\rm AJ}$, $\gamma_{\rm x}$, $\gamma_{\rm y}$	growth ratios of parameters, dimensionless
$ ilde{ u}(heta_i)$	allowance evacuation speed, m/s
p	highest order of data model variables, dimensionless
a_k	coefficient of k-order variable, dimensionless

References

- Adamiec-Wojcik, I., Brzozowska, L., Drag, L., Wojciech, S., 2023. Optimal base motion to compensate for the influence of sea currents during riser re-entry. Mar. Struct. 88, 103357. https://doi.org/10.1016/j.marstruc.2022.103357.
- Ahmed, E.E.E., Demirci, A., 2022. Multi-stage and multi-objective optimization for optimal sizing of stand-alone photovoltaic water pumping systems. Energy 252, 124048. https://doi.org/10.1016/j.energy.2022.124048.
- Ambrose, B.D., Grealish, F., Whooley, K., 2001. Soft hangoff method for drilling risers in ultra deepwater. In: Offshore Technology Conference, April 30—May 3, Houston, Texas. https://doi.org/10.4043/13186-ms.
- Bakker, H., Dunke, F., Dunke, S., 2020. A structuring review on multi-stage optimization under uncertainty: aligning concepts from theory and practice. Omega 96, 102080. https://doi.org/10.1016/j.omega.2019.06.006.
- Bayik, B., Omenzetter, P., Dominic, A.v.d.A., Pavlovskaia, E., 2020. Experimental modelling of a top-tensioned riser for vibration-based damage detection. Eng. Struct. 223, 111139. https://doi.org/10.1016/j.engstruct.2020.111139.
- Cao, Y.Q., Xu, Q., Yu, H.Y., Huang, B., Liu, T.Y., Guo, L.J., 2024. Influence of pipeline diameters and fluid properties on slug frequency in horizontal pipelines. Chem. Eng. Sci. 283, 119397. https://doi.org/10.1016/j.ces.2023.119397.
- Chen, L.M., Chen, G.M., Sun, Y.Y., Jiang, S.Q., Chang, Y.Q., Xu, L.B., 2012. Dynamic and length optimization of typhoon-avoidance evacuation for deepwater drilling risers. The Ocean Engineering 2, 26–31. https://doi.org/10.16483/j.issn.1005-9865.2012.02.003 (in Chinese).
- Dou, Z.J., Liu, Y.S., Qin, X., Gao, D.L., Yang, G.S., 2022. Multi-objective optimization design of deviation-correction trajectory considering the production loss in shale gas cluster well. Petrol. Sci. 19, 2995–3003. https://doi.org/10.1016/ i.petsci.2022.09.024.
- Elsas, J.H., Casaprima, N.A.G., Cardoso, P.H.S., Menezes, I.F.M., 2021. Bayesian optimization of riser configurations. Ocean Eng 236, 109402. https://doi.org/10.1016/j.oceaneng.2021.109402.
- Fan, H.H., Li, C.W., Wang, Z.M., Xu, L.B., Wang, Y., Feng, X., 2017. Dynamic analysis of a hang-off drilling riser considering internal solitary wave and vessel motion. J. Nat. Gas Sci. Eng. 37, 512—522. https://doi.org/10.1016/j.jngse.2016.12.003.
- Gong, K., Lei, C., Dong, Z.C., Zhao, Z.J., Xiong, J.J., Qi, L., 2021. Simulation design of tiny pressure sensor based on least squares data fitting. Chin. J. Sensors Actuators 34 (10), 1320–1325. https://doi.org/10.3969/j.issn.1004-1699.2021.10.007 (in Chinese)
- Hong, A.Y., Xu, Q., Jiang, S.Z., Li, X.Y., Liu, Q.M., Guo, L.J., 2024. Experimental study of interface behavior and sound pressure oscillation of direct contact condensation of a steam jet in flowing water. Exp. Therm. Fluid Sci. 150, 111054. https:// doi.org/10.1016/j.expthermflusci.2023.111054.
- Ja'e, I.A., Ali, M.O.A., Yenduri, A., Nizamani, Z., Nakayama, A., 2022. Optimization of mooring line parameters for offshore floating structures: a review paper. Ocean Eng 247, 110644. https://doi.org/10.1016/j.oceaneng.2022.110644.
- Ju, S.D., Chang, Y.J., Chen, G.M., Chen, L.M., Xu, L.B., 2012. Determination of the hangoff window for deepwater drilling riser. Acta Petrol. Sin. 33 (1), 133–136.

- https://doi.org/10.7623/syxb201201019 (in Chinese).
- Kawano, A., Zine, A., Morooka, C., Ichchou, M., 2021. Analysis of the vibration of risers considering coupled longitudinal and transversal displacements and a new numerical approach. Ocean Eng 222, 108575. https://doi.org/10.1016/ j.oceaneng.2021.108575.
- Klaycham, K., Athisakul, C., Chucheepsakul, S., 2020. Large amplitude vibrations of a deepwater riser conveying oscillatory internal fluid flow. Ocean Eng 217, 107966. https://doi.org/10.1016/j.oceaneng.2020.107966.
- Liu, J., Wang, P.C., Guo, X.Q., Dai, L.M., He, Y.F., 2022a. Nonlinear vibration model and response characteristic of drilling risers in deep-sea under soft suspension evacuation condition. Mech. Syst. Signal. Pr. 169, 108783. https://doi.org/ 10.1016/j.ymssp.2021.108783.
- Liu, J., Zhang, H.S., Gu, C.W., Li, M.B., Liu, Z.L., Zhang, C.J., Wang, Z.K., 2021a. Selection and design of typhoon prevention riser suspension device for deepwater drilling. China Offshore Oil Gas 33 (1), 133–139. https://doi.org/10.11935/ j.issn.1673-1506.2021.01.016 (in Chinese).
- Liu, J.P., Ma, X.W., Zhang, X.Q., Zhang, Z.X., Liu, G.H., 2022b. Axial vibration of deep-water drilling risers under lifting conditions. J. Petrol. Sci. Eng. 209, 109903. https://doi.org/10.1016/j.petrol.2021.109903.
- Liu, X.Q., Chen, G.M., Chang, Y.J., Fu, J.J., Ji, J.Q., 2017. Weak point and operation analysis of deepwater drilling riser system in typhoon condition. In: The 27th International Ocean and Polar Engineering Conference, June 25–30, San Francisco, USA.
- Liu, X.Q., Li, Y.W., Zhang, N., Sun, H.X., Chang, Y.J., Chen, G.M., Xu, L.B., Sheng, L.X., 2020. Improved axial dynamic analysis of risers based on finite element method and data-driven models. Ocean Eng 214, 107782. https://doi.org/10.1016/ i.oceaneng.2020.107782.
- Liu, X.Q., Sun, H.X., Yu, M.R., Qiu, N., Li, Y.W., Liu, F.L., Chen, G.M., 2021b. Mechanical analysis of deepwater drilling riser system based on multibody system dynamics. Petrol. Sci. 18, 603–617. https://doi.org/10.1007/s12182-020-00506-1.
- Liu, X.Q., Wang, X.L., Jiang, Y., Chen, G.M., Xu, L.B., Li, C.W., 2019. An optimization method for the suppression device configuration of risers. Ocean Eng 194, 106619. https://doi.org/10.1016/j.oceaneng.2019.106619.
- Liu, X.Q., Zheng, J., Fu, J.J., Ji, J.Q., Chen, G.M., 2018. Multi-level optimization of maintenance plan for natural gas pipeline systems subject to external corrosion. J. Petrol. Sci. Eng. 50, 64–73. https://doi.org/10.1016/j.jngse.2017.11.021.
- Mao, L.J., Zeng, S., Liu, Q.Y., 2019. Dynamic mechanical behavior analysis of deep water drilling riser under hard hang-off evacuation conditions. Ocean Eng 183, 318–331. https://doi.org/10.1016/j.oceaneng.2019.05.014.
- Meng, S., Chen, Y., Che, C.D., 2020. Coupling effects of a deep-water drilling riser and the platform and the discharging fluid column in an emergency disconnect scenario. China Ocean Eng. 34 (1), 21–29. https://doi.org/10.1007/s13344-020-0003-y.
- Monteiro, B.D.F., Baioco, J.S., Albrecht, C.H., Lima, B.S.L.P.d., Jacob, B.P., 2021. Optimization of mooring systems in the context of an integrated design methodology. Mar. Struct. 75, 102874. https://doi.org/10.1016/j.marstruc.2020.102874.
- Nguyen, T.C., Al-Safran, E., 2021. Marine riser failure analysis for offshore conventional drilling and managed pressure drilling operations. J. Petrol. Sci. Eng. 199,

- 108307. https://doi.org/10.1016/j.petrol.2020.108307.
- Qi, M.S., Li, L.Q., Song, L.S., Cheng, Y.M., Wang, D.B., Zhang, X.F., 2015. Configuration and operation optimization of deepwater drilling riser considering of evacuation due to typhoon. In: The Twenty-Fifth International Ocean and Polar Engineering Conference, June 21–26, Big Island. Hawaii, USA.
- Qiu, N., Liu, X.Q., Liu, Z.W., Li, Y.W., Hu, P.J., Chang, Y.J., Chen, G.M., 2023. Mechanical model and characteristics of deep-water drilling riser-wellhead system under internal solitary waves. Mar. Struct. 90, 103439. https://doi.org/10.1016/ i.marstruc.2023.103439.
- Qu, Y., Wang, P.G., Fu, S.X., Zhao, M., 2023. Vortex-induced vibrations of a top tensioned riser subjected to flows with spanwise varying directions. Int. J. Mech. Sci. 242, 107954. https://doi.org/10.1016/j.ijmecsci.2022.107954.
- Saruhashi, T., Sawada, I., Kyo, M., Miyazaki, E., Yamazaki, Y., Yokoyama, T., Bhalla, K., Stahl, M.J., Ganpatye, A., Han, Y., Gong, L., 2014. Planning and feedback for deepwater drilling riser operation in high currents, typhoons and cold front. In: Offshore Technology Conference, May 5–8, Texas, USA. https://doi.org/10.4043/25187-ms
- Sheng, L.X., Xu, L.B., Liu, J., Jiang, S.Q., Zhou, J.L., 2019. A new conceptual design for suspending drilling riser system. The Ocean Engineering 37 (5), 99–106. https://doi.org/10.16483/j.issn.1005-9865.2019.05.011 (in Chinese).
- Sinha, M., Biswas, S., Biswas, S., 2023. Genetic algorithm and deep learning models compared for swell wave height prediction. Dynam. Atmos. Oceans 102, 101365. https://doi.org/10.1016/j.dynatmoce.2023.101365.
- Song, Y., Yang, J., Zhou, B., 2019. Optimal route design of adjacent wells and mechanical properties of hang-off drilling riser in ocean environment. Int. J. Environ. Sci. Te. 16 (9), 5073–5078. https://doi.org/10.1007/s13762-018-2006-2.
- Sun, Y.Y., Chen, G.M., Chang, Y.J., Ju, S.D., 2009. Hang-off dynamic analysis and the discuss of typhoon-avoidance strategy for ultra-deepwater drilling risers. China offshore platform 24 (2), 29–32. https://doi.org/10.3969/j.issn.1001-4500.2009.02.006 (in Chinese).
- Wang, J.L., 2023. Sea trial investigation for dynamic load compensation effect evaluation on novel soft hang-off system. Ships Offshore Struc 18 (3), 349–357. https://doi.org/10.1080/17445302.2022.2052473.
- Wang, L., Yao, Y.D., Luo, X.D., Adenutsi, C.D., Zhao, G.X., Lai, F.P., 2023a. A critical review on intelligent optimization algorithms and surrogate models for conventional and unconventional reservoir production optimization. Fuel 350, 128826. https://doi.org/10.1016/j.fuel.2023.128826.
- Wang, R.Y., Chen, G.M., Zhang, N., Zhang, H.R., 2023b. Study on storm evacuation operations in deep-sea mining. Ocean Eng 281, 114690. https://doi.org/10.1016/i.oceaneng.2023.114690.
- Wang, S.W., Xu, X.S., Lu, S., 2016. Movement optimization of freely-hanging deepwater risers in reentry. Ocean Eng 116, 32–41. https://doi.org/10.1016/ j.oceaneng.2016.02.029.
- Wang, Z.K., Zhang, Y.T., Wang, R.F., Chen, J.K., Xu, L.B., Liu, J., Huang, L.M., 2021.

- Design and simulation research of riser flexible hang-off system based on variable damping for drilling platform to avoid typhoon. Ocean Eng 236, 109576. https://doi.org/10.1016/j.oceaneng.2021.109576.
- Wu, T.T., Zhao, H., Gao, B.X., Meng, F.B., 2021. Structural optimization strategy of pipe isolation tool by dynamic plugging process analysis. Petrol. Sci. 18, 1829–1839. https://doi.org/10.1016/j.petsci.2021.09.010.
 Xu, L.B., Wang, J.L., Li, Y.W., Sheng, L.X., Li, C.W., Liu, J., Li, M.B., Liu, X.Q., 2022.
- Xu, L.B., Wang, J.L., Li, Y.W., Sheng, L.X., Li, C.W., Liu, J., Li, M.B., Liu, X.Q., 2022. Development and sea trial investigation for deepwater drilling riser specialized soft hang-off system during transit. Ocean Eng 243, 110310. https://doi.org/ 10.1016/i.oceaneng.2021.110310.
- Xu, L.B., Zhou, J.L., Wang, R.Y., Jiang, S.Q., Sheng, L.X., 2015. Analysis of deep water drilling platform evacuation from imminent typhoons with riser hang-off in South China Sea. China Offshore Oil Gas 27 (3), 101–107. https://doi.org/ 10.11935/j.issn.1673-1506.2015.03.016 (in Chinese).
- Yan, Y.M., Liang, Y.T., Zhang, H.R., Zhang, W., Feng, H.X., Wang, B.H., Liao, Q., 2019. A two-stage optimization method for unmanned aerial vehicle inspection of an oil and gas pipeline network. Petrol. Sci. 16, 458–468. https://doi.org/10.1007/ s12182-019-0305-y.
- Yang, C., Liu, Y., Du, J.B., Cheng, Z.B., Wang, H., 2023. Nonlinear dynamic optimization of marine riser system anti-recoil under a flexible multibody framework. Ocean Eng 281, 114666. https://doi.org/10.1016/j.oceaneng.2023.114666.
- Yang, H.Z., Xiao, F., 2021. Multi-objective optimization analysis of ultra-deep water drilling riser under harsh environmental conditions. In: The 31st International Ocean and Polar Engineering Conference. June 20–25, Rhodes, Greece. https:// doi.org/10.1115/omae2018-78559.
- Yang, J., Li, L., Yang, Y.X., Zhang, M.H., 2023. Research on stability of deepwater drilling riser system in freestanding mode. Ocean Eng 279, 114439. https:// doi.org/10.1016/j.oceaneng.2023.114439.
- Yu, H.Y., Xu, Q., Cao, Y.Q., Huang, B., Wang, H.X., Guo, L.J., 2023. Characterizations of gas-liquid interface distribution and slug evolution in a vertical pipe. Petrol. Sci. 20, 3157–3171. https://doi.org/10.1016/j.petsci.2023.03.009.
- Yu, R.F., Diao, B.B., Gao, D.L., 2022. A calculation model for improving the relative borehole uncertainty based on the least square method in relief well. J. Petrol. Sci. Eng. 217, 110863. https://doi.org/10.1016/j.petrol.2022.110863.
- Sci. Eng. 217, 110863. https://doi.org/10.1016/j.petrol.2022.110863.

 Zhang, H.C., Tong, L.L., Addo, M.A., Liang, J.J., Wang, L.J., 2020. Research on contact algorithm of unbonded flexible riser under axisymmetric load. Int. J. Pres. Ves. Pip. 188, 104248. https://doi.org/10.1016/j.jipvp.2020.104248.
- Pip. 188, 104248. https://doi.org/10.1016/j.ijpvp.2020.104248.

 Zhang, W., Zhang, B.L., Han, Q.L., Sun, Y.T., Ji, Y., Zhang, D.W., Zhang, X.M., 2023.

 Observer-based dynamic optimal recoil controller design for deepwater drilling riser systems. Ocean Eng 267, 113324. https://doi.org/10.1016/j.oceaneng.2022.113324.
- Zheng, Q., Chang, H.C., Liu, Z.Y., Feng, B.W., Jian, W., Wei, X., 2023. Design knowledge extraction framework and its application in multi-objective ship optimization. Ocean Eng 280, 114782. https://doi.org/10.1016/j.oceaneng.2023.114782.